AGU PUBLICATIONS

JGR

Journal of Geophysical Research: Space Physics

RESEARCH ARTICLE

10.1002/2016JA022503

A 17 June 2011 polar jet and its presence in the background solar wind

H.-S. Yu[1], B.V. Jackson[1], Y.-H. Yang[2], N.-H. Chen[3], A. Buffington[1], and P. P. Hick[1]

[1]Center for Astrophysics and Space Sciences, University of California at San Diego, La Jolla, California, USA, [2]Institute of Space Science, National Central University, Taoyuan, Taiwan, [3]Korea Astronomy and Space Science Institute, Daejeon, Korea

Key Points:

- An extreme speed jetting feature is observed from three spacecraft perspective views
- The jetting response is shown for the first time in both IPS and SMEI 3-D reconstructions
- The 3-D relationship between surface brightness and the jet response, as well as the associated field changes, is documented

Correspondence to:
H.-S. Yu,
hsyu@ucsd.edu

Citation:
Yu, H.-S., B. V. Jackson, Y.-H. Yang, N.-H. Chen, A. Buffington, and P. P. Hick (2016), A 17 June 2011 polar jet and its presence in the background solar wind, *J. Geophys. Res. Space Physics*, *121*, 4985–4997, doi:10.1002/2016JA022503.

Received 5 FEB 2016
Accepted 20 MAY 2016
Accepted article online 23 MAY 2016
Published online 17 JUN 2016

Abstract High-speed jet responses in the polar solar wind are enigmatic. Here we measure a jet response that emanates from the southern polar coronal hole on 17 June 2011 at the extreme speed of over 1200 km/s. This response was recorded from the Sun-Earth line in Solar Dynamics Observatory/Atmospheric Imaging Assembly (SDO/AIA) and Large Angle and Spectrometric Coronagraph/C2 and both Solar TErrestrial RElations Observatory Extreme Ultraviolet Imager and COR2 coronagraphs when the three spacecraft were situated ~90° from one another. These certify the coronal 3-D location of the response that is associated with an existing solar plume structure and show its high speed to distances of over 14 R_S. This jetting is associated with magnetic flux changes in the polar region as measured by the SDO/Helioseismic and Magnetic Imager instrumentation over a period of several hours. The fastest coronal response observed can be tracked to a time near the period of greatest flux changes and to the onset of the brightest flaring in AIA. This high-speed response can be tracked directly as a small patch of outward moving brightness in coronal images as in Yu et al. (2014) where three slower events were followed from the perspective of Earth. This accumulated jet response has the largest mass and energy we have yet seen in 3-D reconstructions from Solar Mass Ejection Imager observations, and its outward motion is certified for the first time using interplanetary scintillation observations. This jet response is surrounded by similar high-speed patches, but these are smoothed out in Ulysses polar measurements, we speculate about how these dynamic activities relate to solar wind acceleration.

1. Introduction

Solar wind observations of *Ulysses* [*McComas et al*., 1998a] show the polar regions to be uniform and nonstructured during solar minimum [*Phillips et al*., 1994, 1995; *McComas et al*., 1998b, 2008]. This changes near solar maximum, however, to include a complicated mixture of solar wind flows from various sources [*McComas et al*., 2002]. In both cases, close to the solar surface, polar coronal regions contain rapidly varying chromospheric and coronal structures, such as spicules, macrospicules, and jets, as does the rest of the Sun [e.g., *Shibata*, 1982; *Canfield et al*., 1996; *Shimojo et al*., 1996; *Wang et al*., 1998; *Shimojo and Shibata*, 2000; *Cirtain et al*., 2007; *Raouafi et al*., 2008; *Nisticò et al*., 2009; *Liu et al*., 2011; *Tian et al*., 2011; *Yu et al*., 2014]. Using *Hinode* X-ray Telescope (XRT) observations [*Golub et al*., 2007; *Kosugi et al*., 2007], *Cirtain et al.* [2007] find two speeds for jet outflow components: one is slow, near the sound speed, and the faster speed is comparable to the low-corona Alfvén velocity. These two components are also mapped in Coronal Multichannel Polarimeter (CoMP) [*Tomczyk et al*., 2008] polar coronal hole and closed-field observations near the solar surface [*Jiang et al*., 2007; *Tomczyk and McIntosh*, 2009; *Threlfall et al*., 2013; *Liu et al*., 2014]. These high speeds are generally not associated with a jetting response.

The relationship between EUV jets observed by the Solar TErrestrial RElations Observatory (STEREO) Sun-Earth Connection Coronal and Heliospheric Investigation (SECCHI) Extreme Ultraviolet Imager (EUVI) [*Howard et al*., 2008] and Hinode polar X-ray jets has been studied by *Raouafi et al.* [2008]. They find that both types of jets have similar characteristics. Additionally, they find that a haze of outward flowing plasma can follow them for up to several hours. *Wilhelm et al.* [2011] review jet response observed by white light coronagraphs and associate their outflow with either the onsets or brightness enhancements of polar plumes. *Wang et al.* [1998] determine that plume enhancements in white light associated with EUV flaring bright-point jets within coronal holes can have speeds greater than 1000 km/s, as measured by the Large Angle Spectrometric COronagraph (LASCO) C2 coronagraph [*Brueckner et al*., 1995] on board the Solar and Heliospheric Observatory (SOHO). This indicates that a flow of associated plasma material continues after the jet initiation and appearance of the bright point. *Jackson et al.* [2014] also report that the bulk outward solar wind motion over the polar regions can vary by as much as an order of magnitude, with the variation correlated to brightness.

Observation of flaring X-ray bright points seen over the entire solar disk has a longer history [e.g., *Vaiana et al*., 1970; *Krieger et al*., 1971], and X-ray jetting outflow is often associated with these bright points. When near the solar polar regions, these usually are isolated temporally and spatially from other features. In any case this outflow is usually attributed to magnetic reconnection between an existing ambient coronal magnetic field and emergence of new bipolar fields at that location [e.g., *Shibata et al*., 1992; *Canfield et al*., 1996; *Raouafi et al*., 2008; and also see the review by *Schmieder et al*., 2014]. *Isobe et al.* [2005] also found that given the magnetic Rayleigh-Taylor instability, the resultant thin current sheets in the emerging magnetic fields may lead to spatially intermittent reconnection. From XRT images, *Savcheva et al.* [2007] report 60 or more large jets per day, and that these eject considerable mass into the corona. Recently, upon tracing high-speed polar jets over a large spatial scale outward into the heliosphere from the perspective of Earth, *Yu et al.* [2014] show that all solar jets combined contribute totals of ~3.2% of the solar wind mass and ~1.6% of its energy. However, these densities and energies of the largest jets are generally 10 times larger than estimates for jets observed in X-rays near the solar surface [*Shibata et al*., 1992; *Shimojo and Shibata*, 2000; *Corti et al*., 2007; *Glesener et al*., 2012]. Prior to the *Yu et al.* [2014] analyses, the plasma measurements from jetting had not previously incorporated observations in the interplanetary medium.

The present article continues this line of investigation but from the perspective views of three spacecraft situated ~90° from one another. Here we trace the response of a high-speed solar jet on 17 June 2011, the fastest and largest we have observed to date, from above the south pole into the inner heliosphere and reconstruct its three-dimensional (3-D) structure for the first time using interplanetary scintillation (IPS) and Solar Mass Ejection Imager (SMEI) observations. Because we can view the jetting response and place it precisely in a 3-D context, we now know its exact speed and track into the heliosphere. Traced back to near the solar surface, this allows further investigation of its relationship to the evolution of oppositely directed polar magnetic field and changing EUVI and Atmospheric Imaging Assembly (AIA) brightness near the Sun. We also discuss the presence of this very energetic response in the background solar wind and its relationship to other fast structures observed near its polar location. Section 2 presents the data and describes the analysis that traces this jet into the heliosphere. Section 3 presents the two-dimensional (2-D) correlation speed maps showing this jet's response and its relationship to the background solar wind. Section 4 discusses a possible mechanism of this jetting activity and its continuing presence at large solar distances. We summarize in section 5.

2. The Large Jet on 17 June 2011

The Hinode Observing Proposal (HOP-187) collected data from spacecraft and ground-based instruments to study polar jets and to trace their response into the heliosphere [*Jackson et al*., 2011b]. These observations utilize all of the spacecraft and ground-based information available during the HOP-187 periods on 17 June and 22 August 2011. XRT and the *Atmospheric Imaging Assembly* on board *Solar Dynamics Observatory* (SDO/AIA) [*Lemen et al*., 2012] together observed the jet responses from the solar surface to inner corona, SOHO/LASCO C2 [*Brueckner et al*., 1995] observed the outer corona with deep exposures and much better temporal resolution, and STEREO/SECCHI COR2 [*Howard et al*., 2008] in turn provided data from east and west of the Sun. Finally, data from the IPS system in Nagoya, Japan [*Kojima and Kakinuma*, 1987; *Tokumaru et al*., 2011] and in Ooty, India [*Manoharan*, 2010] and from the SMEI [*Eyles et al*., 2003; *Jackson et al*., 2004] enabled tracing the jets into the inner heliosphere. Combining all these near-simultaneous observations, we have derived the 3-D configurations of the transient structures in the solar polar regions.

One of the fastest jet responses we have found to date occurred in the southern polar region on 17 June 2011 and was observed by AIA, LASCO C2, and STEREO COR2 coronagraphs. SDO/AIA was launched on 11 February 2010 to provide unprecedented views of the corona with fine temporal and spatial resolution in multiple wavelengths, near simultaneously. The full-disk images have a cadence of 12 s and spatial resolution of ~1.5 arc sec [see *Lemen et al*., 2012]. SOHO/LASCO and STEREO/COR2, launched in 1995 and 2006, respectively, observe the outer corona with fields of view starting from ~2 R_S. STEREO was designed to view the 3-D heliosphere using an unprecedented combination of imaging mounted on virtually identical spacecraft flanking the Earth in its orbit [see *Howard et al*., 2008]. Figure 1a shows the observed jet response in AIA 304 Å at 2:55 UT. This activity lasted for about 90 min (see Figure 10 in section 4 for a time series plot of AIA brightness). Bright-point intensities in AIA at 304 Å began at 2:27 UT, reached a small first peak at 2:35 UT, and its

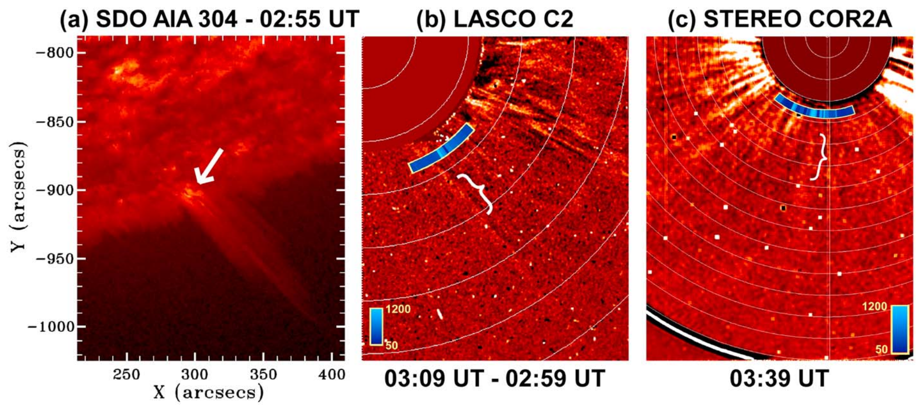

Figure 1. The large jetting activity observed on 17 June 2011, by SDO/AIA and coronagraphs, shown here with coordinates centered upon the Sun. (a) AIA at 304 Å. This clearly shows bright loop structures (white arrow) near the surface and open structures extending to the outer corona. (b) C2 running difference image. (c) COR2-A smoothed background-subtracted image. C2 and COR2-A images have a blue-colored band presenting speeds from a 2-D correlation using the immediately following image [see *Yu et al*., 2014]. The blue image bar at the lower corner indicates the displayed range of speeds. The white curly bracket marks the location of jet response. White concentric circles mark increments of 1 R_S from the Sun center.

maximum at 3:04 UT. The brightening process recurred several times and ended after 4:00 UT. Loop structures associated with the jetting appeared at 2:44 UT. Figures 1b and 1c show this response in C2 and COR2-A coronagraphs. In C2 running-difference images (these images have an average base subtracted that extends over about 6 h), the jet response shows as a bright enhancement propagating southwest along a preexisting plume structure in the southern corona hole region at a fairly high speed. At a nearly simultaneous onset time, but 90° away from the Sun-Earth line, COR2-A observed this bright structure at greater height propagating outward in the southeast direction at approximately the same speed.

This large jet response can easily be tracked directly in these C2 and COR2-A images. When tracing back at constant speed, it has an onset on the solar surface at $R_S \approx 1.0$ within minutes of the brightest EUV jetting in AIA. Figure 2 shows the outward track of the centroid of this jet response observed in coronagraph images. The averaged radial extent of the outward moving structure is about 1.2 R_S. These are determined by following faint increased-brightness features that move consistently outward from one image to the next. The

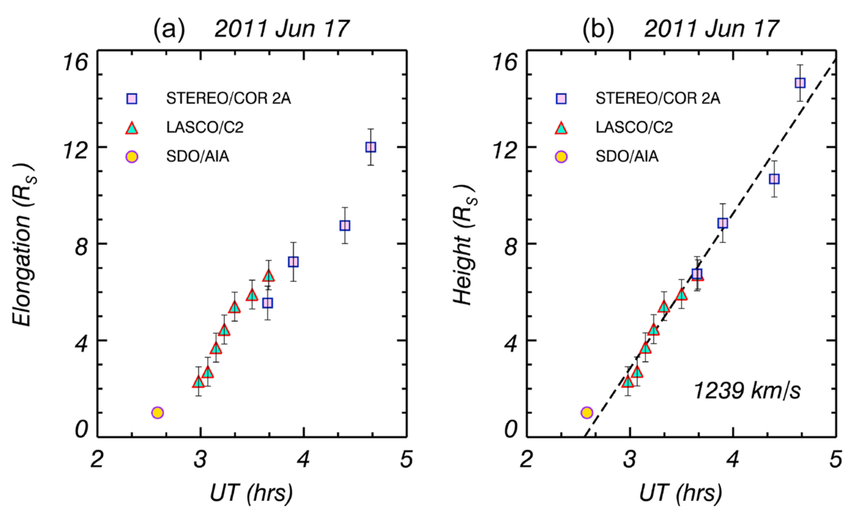

Figure 2. (a) The 17 June plot of elongation versus time and (b) of R_S solar distance with time of the centroid of the jet response shown in Figure 1. The dashed line in Figure 2b is a least squares fit at the indicated speed. The circle marks the onset (see first peak time of brightness in time series plot in Figure 10) of the jet response in AIA 304 Å. Triangles and squares, respectively, mark observations from LASCO C2 and COR2-A. The radial extent of the outward moving structure is indicated by vertical bars.

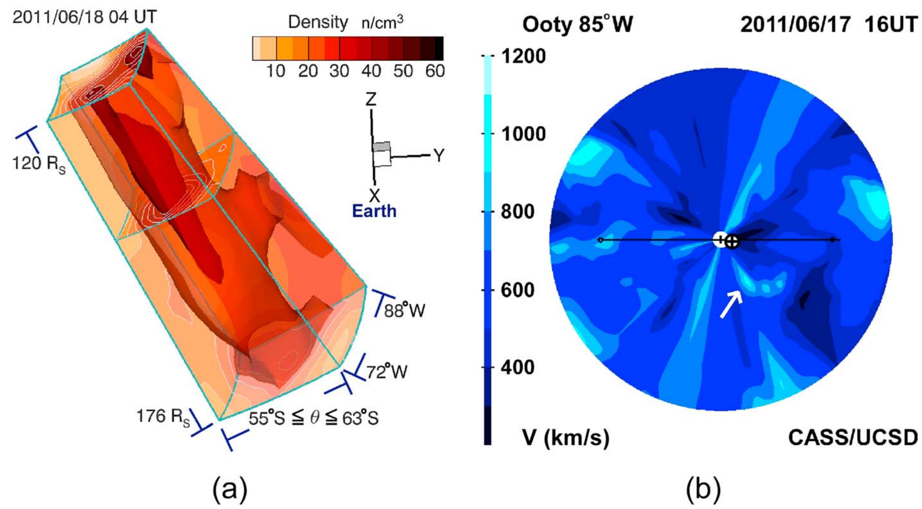

Figure 3. Density and velocity plots. (a) Isolation of the jet-response density, from 3-D reconstruction of SMEI data, during its outward motion. The jet is shown at a distance larger than 120 R_S away from Sun center on 18 June 2011. An r^{-2} density fall-off is removed from these volumes to present their values over solar distance with comparable volume and density ranges. (b) An IPS meridional cut 3-D velocity presentation of the jet response at 16:00 UT on 17 June. The white arrow points out this high-speed structure, observed at 85° west of the Sun-Earth line. More high-speed material propagates ahead of this jet. The circle with cross marks the Earth, and the solid line shows Earth's orbit projected on the plane of the meridional cut.

determinations of the outward speed have errors of about 15%. When considering this structure in 3-D, we correct its location in the plane of the sky (elongation versus time) to its out-of-the-sky-plane motion (height versus time) using a triangulation method. The least squares fitted jet response true speed is greater than 1200 km/s and exhibits no apparent deceleration out to 14 R_S.

Remotely sensed IPS and Thomson-scattering observations from SMEI have provided a primary source of data to study the physics and global properties of heliospheric structures. These are relatively stable as streamer and corotating interaction regions or are transient as coronal mass ejections (CMEs) and their interplanetary counterparts (interplanetary coronal mass ejections). A 3-D time-dependent tomographic technique using these remotely sensed data has been developed by *Jackson et al.* [2001, 2003, 2010, 2011a, and references therein] to reconstruct a volumetric map of density and velocity nearly complete over the whole inner heliosphere with a time cadence of half to 1 day. The tomographic technique employs multiple remotely sensed line-of-sight data from a single observing location, i.e., Earth, and then iteratively fits a pure kinematic solar wind model to these data to reconstruct the heliospheric structures as they propagate through the inner heliosphere to Earth and beyond. Adding in situ measurements, when available, further enhances the remote sensing determination at Earth. This 3-D reconstruction process permits not only isolation of enhanced density structures from the surrounding heliosphere but also determines their 3-D extent. These SMEI and IPS tomographic analyses also provide 2-D images of structures to quantitatively measure 3-D mass and energy of those features that have been identified in the images. SMEI data have been processed to remove aurora, and high-energy particle hits [*Jackson et al.*, 2004, 2008; *Hick et al.*, 2005, 2007; *Mizuno et al.*, 2005] now at image resolutions of 1°. As in *Yu et al.* [2014] the resulting larger quantity and quality of data are used here for the high-resolution tomographic measurements of volume, density, and energy of the jet response at different solar distances.

This tomography analysis follows the large response associated with AIA-observed jets, tracking them into the SMEI field of view. Figure 3a is a 3-D structure, having a long-term 2 week base removed, that has been isolated from the rest nearby during this period. The jet response has a tube shape and a considerable radial extent. In combination with Ooty IPS velocity observations, the tomographic analysis reconstructs this jet response in a 3-D velocity volume. A 2-D meridional cut from the 3-D volume located at 85° west of the Sun-Earth line (Figure 3b) shows this object at ~0.4 AU moving outward at $>$ 1000 km/s. The location and timing of the high-speed component observed in a combined SMEI and IPS 3-D reconstruction both agree well with those extrapolated from C2 and COR2-A. Further analysis (as in *Yu et al.* [2014]) provides direct manipulation of the volume, and of geometric objects imbedded within it, to separate selected volumetric material

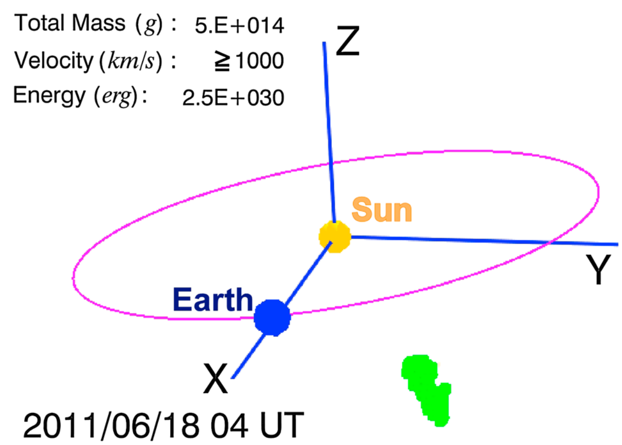

Figure 4. The 3-D-reconstructed analysis of the 17 June jet response observed at 04 UT the following day. The green area marks the isolated volume propagating southwest with a speed higher than 1000 km/s. The determination of this volume element's mass and kinetic energy of outward motion is listed. The volume of this component is ~0.001 AU^3.

within a given 3-D contour interval and determine its mass and energy. The result, similar to those for CMEs [*Jackson et al.*, 2006, 2008] and jets [*Yu et al.*, 2014], is shown in Figure 4 where the jet response is isolated by a 1 AU normalized density contour of 27 Np/cm^3 to separate it from considerable background solar wind material. Total mass of the isolated material within this contour is 5×10^{14} g, and its outward motion kinetic energy is 2.5×10^{30} erg.

3. Coronagraph Speed Observations

Jackson and Hick [1996] and *Jackson et al.* [1998] developed a 2-D cross-correlation-analysis technique to measure coronal outflow, also called "optical flow" [see *Horn and Schunck*, 1981], from consecutive coronagraph images. This was subsequently modified to provide speeds of the coronal jetting response [*Yu et al.*, 2014] and solar wind acceleration [*Jackson et al.*, 2014] using LASCO C2 and STEREO COR2-A data. It derives a speed by selecting a coronagraph image correlation area strip of sky (first image) and then exploring over an area of the following image (second image), limited by an outer boundary. After searching over the second image, the chosen 2-D location of an earlier structure within the correlation box (the yellow square in Figure 5a) is presumed to be the one having highest correlation with a small portion of the strip area in the first image. The 2-D "plane of the sky" speed is the distance between the center of the first area and chosen second area divided by the two-image time interval. By applying this process to each grid of distance and position angle in the correlation area on the first coronagraph image, a "speed map" (Figure 5b) is constructed by assigning the measured speed to the location in the first image.

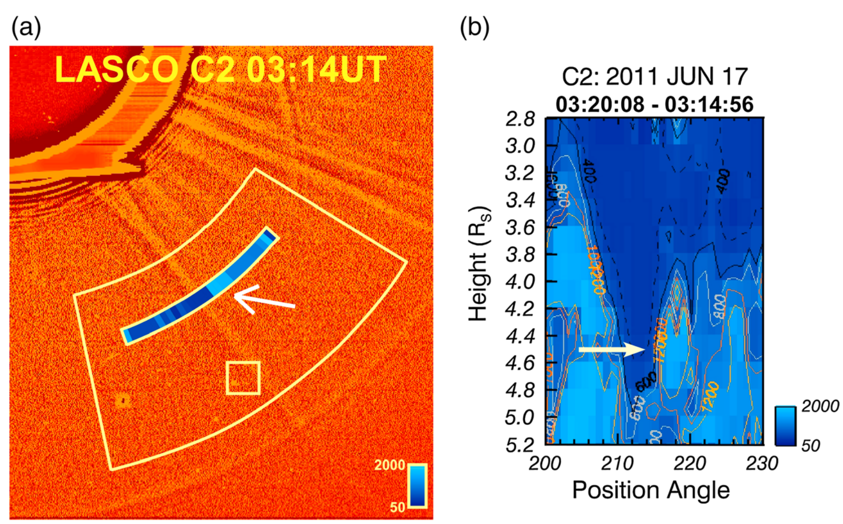

Figure 5. (a) LASCO C2 17 June 2011 background-subtracted image, with superposed blue-colored speed results at 4.4 R_S from the 2-D cross correlation with the next following image. Also shown is the size of the exploratory region (area here bounded by the inner and outer curved lines and yellow radials) to be used in the following image, and the small yellow square indicates the size of the correlation box ($0.4\,R_S \times 0.4\,R_S$). (b) A speed map at different heights and position angles derived by stepping the 0.2 R_S correlation region outward. The constant-speed contours, starting from 400 km/s, refer to 400, 600, 800, 1000, and 1200 km/s. The speed response of this large jet is marked by the arrow and confirms that this feature moves outward at over 1200 km/s. In each panel, the blue bar (lower right) indicates the displayed range of speeds.

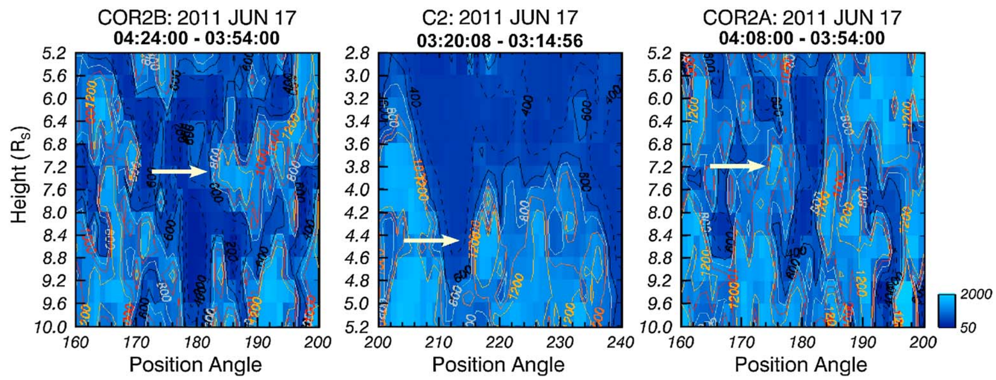

Figure 6. Three 2-D correlation speed maps showing the same jet response observed at ~90° longitude apart. All three speed maps show highly variable solar wind structures with slow and fast patches of material.

The coronagraph images used here are preprocessed by subtracting an average base that extends over about 6 h, a time much longer than the C2 and COR2 image cadence. These images are also smoothed by averaging over ~0.1 $R_S \times 0.1\,R_S$ area. Experiments with several different grid sizes and correlation boxes for the images, *Jackson et al.* [2014] found that a correlation box of ~0.4 $R_S \times 0.4\,R_S$ did not significantly alter the results obtained. We also allowed different speed ranges, from 50 to 1200 km/s and from 50 to 2000 km/s, and minimum correlation requirements and found the locations of these high-speed patches virtually stay the same.

Figure 6 shows speed maps obtained from 2-D correlations of this same 17 June 2011 high-speed response, using data from LASCO C2 and STEREO COR2-A and COR2-B, which are ~90° apart from each other in ecliptic longitude. All three speed maps show a jet response (white arrows in Figure 6) that propagates outward at greater than 1200 km/s and is about 1.2 R_S long and 3° wide. The COR2 speed maps also show irregular patches of high and low speed coronal solar wind structures around the jet response, and this same general solar wind character is seen in the C2 map. When *Jackson et al.* [2014] analyzed both C2 and COR2 coronagraph image pairs having approximately the same start times in 2007, they found a surprising result that polar coronal hole outflows consist of intermittent slow and fast patches of material. Measurements of the mean speed as a function of height for these patchy structures show an average outward acceleration. This acceleration is similar to that obtained for solar wind mass flux determinations of outflow in large polar coronal hole regions [*Munro and Jackson*, 1977; *Kohl et al.*, 1998]. *Jackson et al.* [2014] also found that there is a positive correlation of speed of a coronal patch and its brightness for either C2 or COR2-A in the northern polar region. This conclusion of a high positive correlation of patch speed and brightness holds true here for C2 coronagraphs (Figure 7), and with lower positive correlation for COR2-A and COR2-B during this period. Thus, the present study for 17 June 2011 as in *Yu et al.* [2014] also substantiates the idea that the high-speed regions are generally associated with higher brightness patches in the coronagraphs.

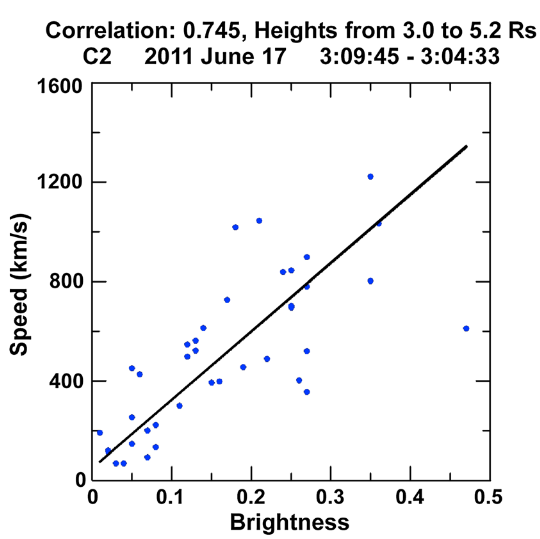

Figure 7. Correlation of coronal-speed patches with their brightnesses in C2 images. The correlation is calculated for the southern polar region, within 3.0 to 5.2 R_S in height, and 160° to 200° in position angle. The associated uncertainty in speed is ~200 km/s.

4. Discussion

We have here traced the large jet that occurred on 17 June 2011 in the southern corona hole region, from the solar surface into the interplanetary

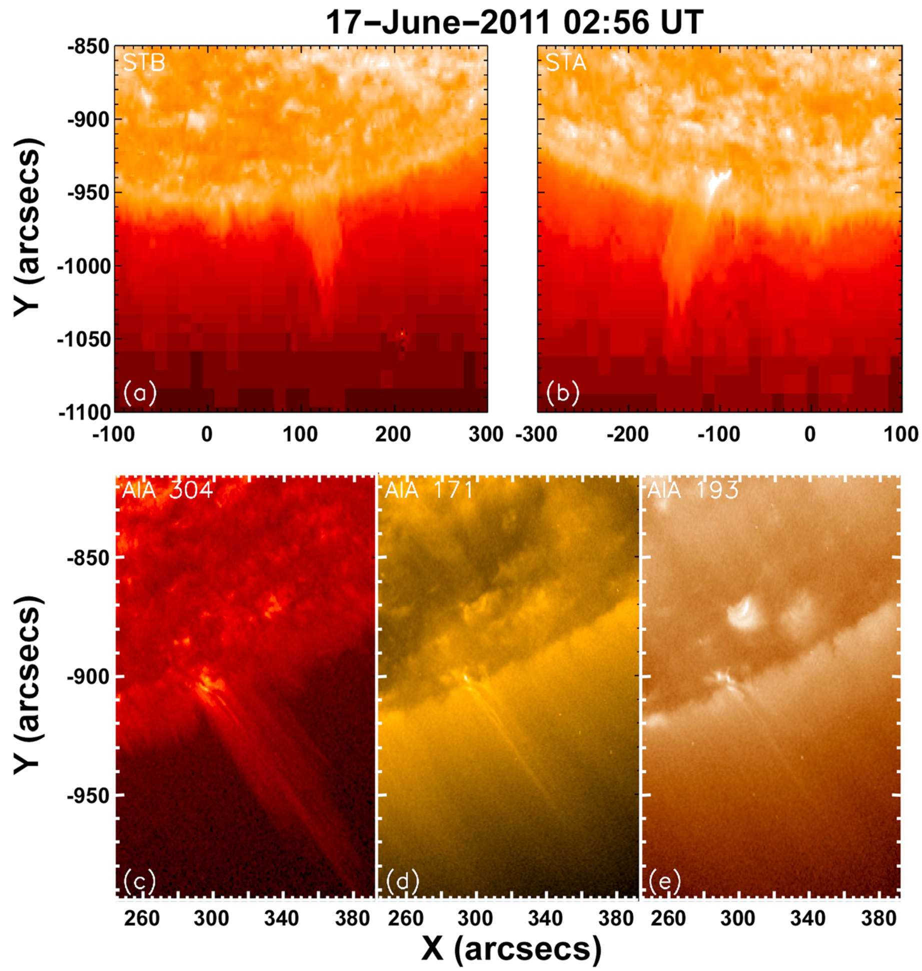

Figure 8. The jet response observed in EUVI-A, EUVI-B, and AIA images. (a) EUVI-B 304 Å, (b) EUVI-A 304 Å, (c) AIA 304 Å, (d) AIA 171 Å, and (e) AIA 193 Å. These images clearly show the jet location and nearby vertically oriented flux tube structures.

medium. This jet response can be tracked in both C2 and COR2 coronagraph images directly and exhibits a fairly high speed. The C2 jet response was observed as a bright enhancement propagating southwest along a preexisting plume structure. This bright enhancement was a short-lived patch of high-speed structure clearly seen in LASCO C2 and STEREO COR2-A and COR2-B speed maps, where C2 and COR2 were ~90° apart from each other in ecliptic longitude. Looking closer to the surface of the Sun (Figure 8), SDO/AIA and STEREO/EUVI also show the solar jet and nearby approximately vertical flux tube structures [*Tsuneta et al.*, 2008]. The jet response moves away from the Sun nonradially relative to its solar surface location. In EUVI-B, only the ejected material is visible. On the opposite side of the Sun, in EUVI-A images, both the bright point at the footpoint region on the surface and the outward ejected material are observed, and together these form an Eiffel Tower shape [*Nisticò et al.*, 2009]. This event is also visible in AIA at 171 Å and 193 Å wavelengths (Figures 8d and 8e). Loop structures and bright points are observed more clearly in AIA images at almost the same time with higher temporal and spatial resolution in multiple wavelengths. The EUVI images confirm that the jet is located and ejected toward the southwest, as seen from Earth, and in the earthward direction.

Figure 9 presents a sequence of AIA images which clearly show a temporal shift of bright points, loop locations, and jet positions. Such a location shift and changes of structure during the whole period of jetting activity suggest an evolution of the magnetic configuration. Magnetic reconfiguration can occur due to magnetic reconnection at different locations on the solar surface [*Shibata et al.*, 1992; *Yokoyama and Shibata*, 1996; *Shimojo et al.*, 1996; *Moreno-Insertis et al.*, 2008; *Shimojo and Tsuneta*, 2009; *Filippov et al.*, 2009; *Pariat et al.*, 2009]. A photospheric sheared flow-induced Kevin-Helmholtz instability [*Karpen et al.*, 1993] may alter the velocity field pattern, which would be reflected in the magnetic field. Magnetic field polarity inversions can

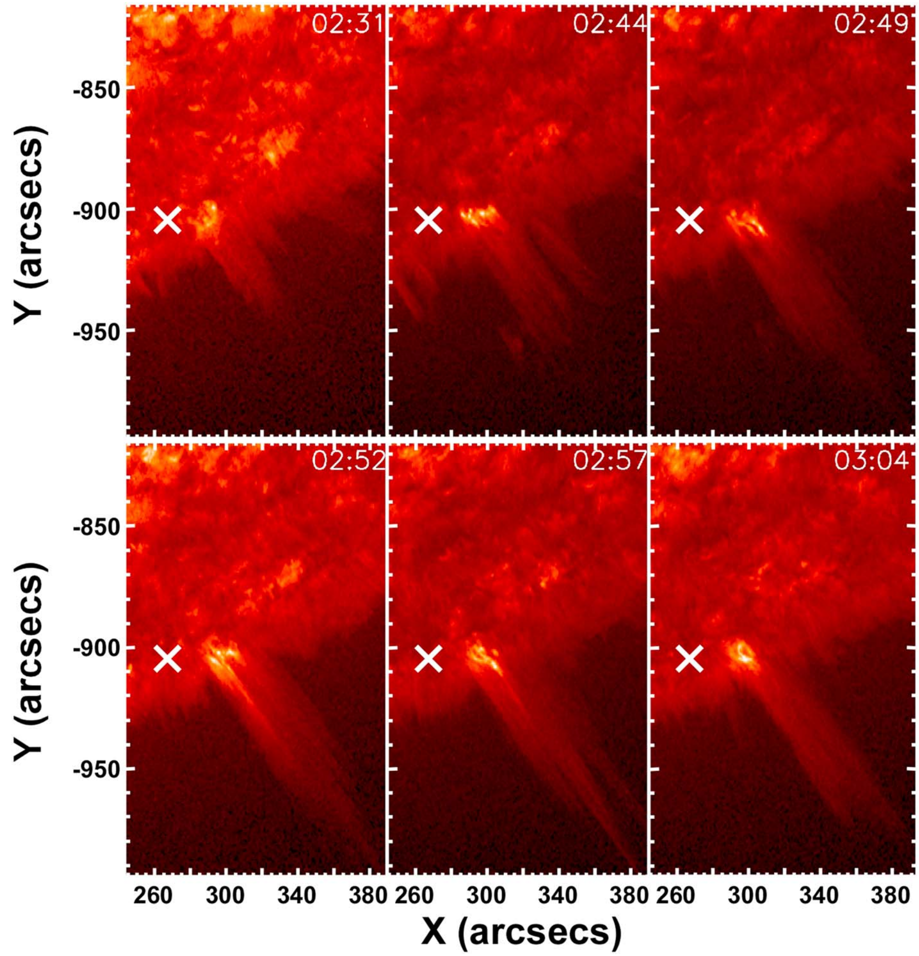

Figure 9. The jet response in a sequence of AIA 304 Å images. During this interval, the jet footpoint changes from bright points to loops and the loops also change direction from northwest-southeast (02:31 UT) to east-west (02:44 UT). During the whole jetting activity period, the jet shape also changes from one type to another, illustrating the dynamic change of magnetic configuration throughout. The white cross provides a fixed reference point.

be driven by radial velocity field structures [*Landi et al*., 2006] or by eruption of macrospicule-size magnetic loops [*Yamauchi et al*., 2004]. All these or perhaps even more complicated combinations have effects on the magnetic reconfigurations. Similar to the results shown in *Nisticò et al.* [2009, 2010], the jet footpoints typically appear as low-coronal bright points or loops, and these two features sometimes seem to coexist. In this event, although the jet structure appears similar in the SECCHI-A and SECCHI-B images 180° from one another, the AIA images show how these features can change in appearance with different wavebands, as well as from a different perspective.

Solar coronal jetting activity is generally attributed to magnetic reconnection between an existing ambient coronal magnetic field and emergence of new bipolar fields at that location [*Shibata et al*., 1992; *Canfield et al*., 1996; *Raouafi et al*., 2008; and also see the review by *Schmieder et al*., 2014]. A recent observation also suggests that the eruption of minifilaments can be the driver of X-ray jets in the polar coronal hole regions [*Sterling et al*., 2015]. *Tsuneta et al.* [2008] describe flux tubes that are vertically oriented, like the ones shown in Figure 8, that have a maximum solar surface average field strength of 1.5 kG. Calling these “kilogauss patches,” they note that these all have the same sign as the polar magnetic field in any given polar region. *Shimojo and Tsuneta* [2009] speculate that the extensions of these flux tubes into interplanetary space may serve as a guiding field for jet response, coronal plume outflow, and fast solar wind. The Helioseismic and Magnetic Imager (HMI) on board SDO [*Scherrer et al*., 2012] provides full-disk high-resolution magnetic field data during this time. These line-of-sight magnetograms show apparent changes in negative magnetic flux in the southern coronal pole positive field at the same location as the EUV jet as denoted by the white box in

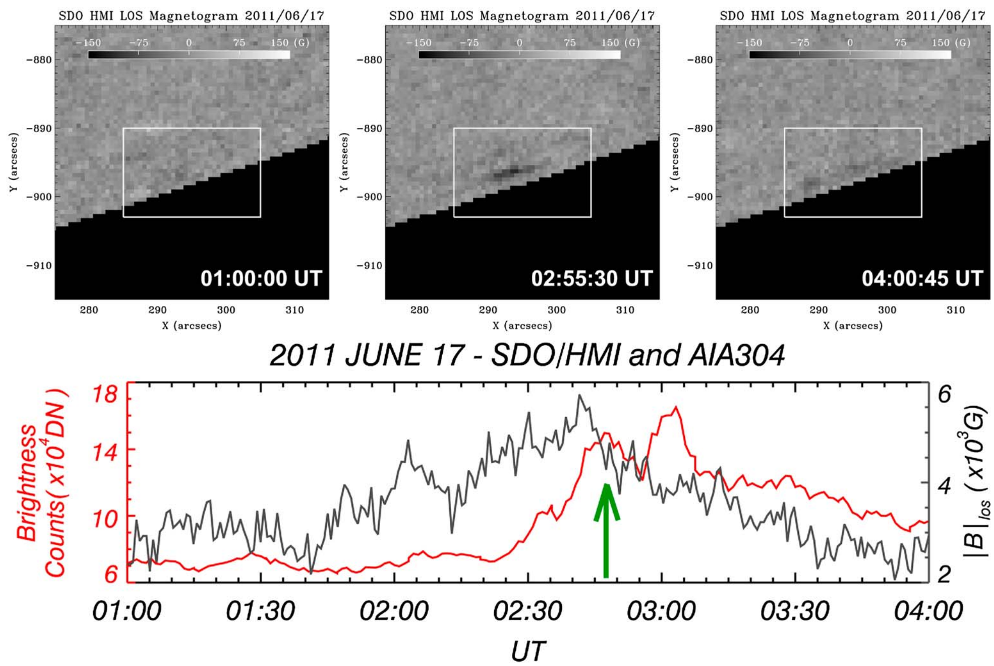

Figure 10. (top row) A sequence of SDO/HMI line-of-sight magnetograms shows apparent changes in opposite polarity flux (negative field) into the southern coronal pole field at the same location as the EUV jet. (bottom) The temporal evolution of the component of magnetic field along the line of sight (with $|B|_{\rm los} > 20$ G) and AIA 304 Å brightness counts at the jetting activity area (within the white box). The green arrow marks the time that AIA brightness counts reach to their first peak after the emerging flux began to diminish.

Figure 10. Negative magnetic field flux started to emerge from the limb of the southern pole at ~1 UT and faded away at ~4 UT. At the same time, the intensity in AIA 304 Å started to increase significantly at 2:25 UT, close to the onset of bright points at the jetting activity footpoints. Note that the AIA brightness counts reach the first peak at ~2:47 UT (green arrow) after the emerging flux begun to diminish. The magnetic field measurement has a large uncertainty near the solar limb due to the slanting perspective. Even so, temporal variations of magnetic flux and AIA brightness in Figure 10 qualitatively confirm a scenario in which the magnetic field emergence is followed by a magnetic field cancelation that could be associated with a jet ejection. [*Heyvaerts et al.*, 1977; *Shibata et al.*, 1992; *Yokoyama and Shibata*, 1995; *Canfield et al.*, 1996; *Jiang et al.*, 2007; *Moreno-Insertis et al.*, 2008; *Raouafi et al.*, 2008; *Yang et al.*, 2011; *Huang et al.*, 2012; *Schmieder et al.*, 2013; *Raouafi and Stenborg*, 2014].

The jet response directly tracked by eye in coronagraph images has an onset time close to the beginning of the bright point activity in EUV image. The jet was tracked as a bright enhancement propagating at speeds of over 1200 km/s which has a direct correspondence in the speed maps obtained from 2-D correlation analyses between successive images. The speed maps also show that the high-speed regions are those of brighter patches and thus of higher density. We thus feel these results that show small bright enhancements in C2, COR2-A, and COR2-B observations 90° in longitude apart have the most likely explanation not as wave phenomena but of actual material flow in the corona. Isolation of this accumulated jet response in SMEI 3-D reconstruction analysis contains the most mass and has the fastest speeds we have analyzed so far. *Yu et al.* [2014] study the September 2007 solar jet responses in Hinode X-ray images as well as LASCO and STEREO coronagraphs. By assuming the amount of mass in a jet response is related to the jet fall-off in brightness with number, they found that solar jets provide only ~3.2% of the total solar wind mass. As in this earlier result, the estimated mass of the present jet is about 10 times larger than the on the solar surface values of the largest jets in previous work [*Shibata et al.*, 1992; *Shimojo and Shibata*, 2000; *Corti et al.*, 2007; *Glesener et al.*, 2012]. However, we can see from Figure 10 that the duration of increase in AIA total intensity of this continuously jetting activity is about 90 min (red curve), which intensifies significantly only after the magnetic flux has begun to diminish. Within this 90 min period, there are successive amounts of outflowing material viewed in the AIA images, and in the coronagraphs, of which only the largest of these enhancements has been carefully documented (in Figures 1, 2, 5, and 6). This is consistent with *Wang et al.* [1998] showing that a sustained associated high-speed plasma material flow follows the jet initiation and bright point occurrence. This also agrees with *Raouafi et al.* [2008] who describe a haze that follows jets for durations of minutes up to several hours indicating plasma outward flow over the interval. At larger distances from the Sun, *Neugebauer* [2012] suggests that large polar X-ray jets can initiate or enhance plumes that result in the *Ulysses*-observed microstream peaks in the solar wind. Thus, we think that the density enhancements in the lower corona (as shown in AIA EUV and coronagraphs) appear to be segmented tracers of a more sustained flow of material which forms what we see in the SMEI heliospheric analyses, as a large elongated density enhancement. In other words, the high-speed dense structure isolated in the SMEI and IPS 3-D reconstructions is most likely a result of the accumulation of the coronal jet responses in the heliosphere over the time of the flux emergence/cancelation.

Because the corona above the polar region is filled with many of these features, observed as segmented high-speed regions associated at the same locations with brighter plasma patches [*Jackson et al*., 2014], we do not feel that this coronal structure is limited to jetting regions as a one-to-one response to the jetting brightness. The jetting makes these features visible in a dramatic way, but the ubiquitious polar presence of these segmented high-speed coronal patches indicates a more general feature of the solar wind which consists of regions of segmented high-speed plasma flow superimposed upon an otherwise slower background. This high-speed flow, as *Tsuneta et al.* [2008] speculate, is almost certainly associated more with the strong magnetic field regions (kilogauss patches) present over the whole polar region on the solar surface than the jetting itself.

Still to be determined is how energy is imparted to these high-speed patches of coronal material, as well as details of how they finally dissipate into the solar wind at large distances from the Sun. If the jet brightness does not indicate the amount of energy imparted to the coronal high-speed patches, over the polar region, then another source of energy beyond jetting must be found for these ubiquitious coronal features. Here the polar observations from CoMP [*Tomczyk et al*., 2007; *Tomczyk and McIntosh*, 2009; *Threlfall et al*., 2013; *Liu et al*., 2014] come to mind that show apparent high-speed enhancements which they assume are associated with an Alfvén flux in polar coronal regions. How this high-speed magnetic change imparts energy to produce the localized high-speed flow in patches seen in the corona must still be worked out, but some of the more popular processes include Alfvén flux heating [*Hollweg,* 1981, 1982, 1992; *Hollweg et al*., 1982; *Tomczyk et al*., 2007; *Tomczyk and McIntosh*, 2009; *McIntosh and De Pontieu*, 2012; *De Moortel et al*., 2014] and/or the production of shocks that drive outward small coronal regions [e.g., *Lee and Wu*, 2000]. Once these high-speed coronal patches are formed they must dissipate over solar distances after imparting their energy to the solar wind. This must happen before 1 AU so that the solar wind observed in coronal hole regions, and especially in Ulysses observations of polar regions during its times of solar minimum passage [*Phillips et al*., 1995; *McComas et al*., 2000, 2008], become the more uniform and less dynamic speed structure observed.

5. Summary

We have tracked a large jet response, which took place on 17 June 2011, in the SDO/AIA observations, through the sky covered by LASCO C2 and STEREO COR2-A and COR2-B coronagraphs, and into the IPS and SMEI fields of view. The coronagraph response directly measured by C2 and COR2-A, when traced back with constant speed to the solar surface, shows a close association to the AIA-observed EUV jet peak brightness onset time. In the speed maps obtained from 2-D correlations, the polar solar wind, especially near the solar surface, shows an extremely dynamic character. Both fast and slow solar wind structures in close proximity can be seen in near-simultaneous images from C2 and in both COR2-A and COR2-B. This same high-speed slightly enhanced material observed 90° in longitude from each other indicates that the jet response is from material flow. A jet response propagating outward at a fairly high speed is also observed in 3-D reconstructions from SMEI and IPS data with the proper timing and at the appropriate 3-D location indicated by the lower corona observations. From a sequence of AIA images and HMI line-of-sight magnetograms, we find that the jet features evolve throughout the evolution of an emerged magnetic field. Therefore, we conclude that the large jetting activity studied here would be associated with an emergence of opposite polarity flux into the southern coronal pole field followed by the cancelation with the surrounding field. The high-speed dense structure isolated in the SMEI and IPS 3-D reconstructions is most likely a result of the accumulation of the coronal jet responses in the heliosphere over the time of the flux emergence/cancelation.

Although the feature tracked shows one incidence of high-speed material associated with the jetting activity, this high-speed coronal patch is by no means unique to this coronal jetting event or even a single time within the period of this jet. These features serve as indicators of the background corona brightness enhancements and indicate an ubiquitous presence in polar coronal regions at perhaps as much as a 100-fold mass and energy value greater than the coronal response itself. This is most likely an indication of the primary mechanism of solar wind acceleration that includes the dissipation of these high-speed, brighter (and thus more dense) solar wind patches.

Acknowledgments
H.-S. Yu, B.V. Jackson, P.P. Hick, and A. Buffington were supported at UCSD by NSF grant AGS-1358399 and NASA grant NNX14AC11G. The authors wish to acknowledge and thank the LASCO coronagraph group for the C2 coronagraph images (http://sharpp.nrl.navy.mil/cgi-bin/swdbi/lasco/img_short/form), the STEREO SECCHI group for making available their COR2 and EUVI images (http://stereo.gsfc.nasa.gov/beacon/), and also the SDO/HMI and SDO/AIA consortia for making the data available (http://sdo.gsfc.nasa.gov/data/). SDO is a mission for NASA's Living With a Star (LWS) Program. SMEI and IPS data used in low-resolution volumetric analyses are available at UCSD (at http://smei.ucsd.edu and http://ips.ucsd.edu/) and at the NASA Goddard Community Coordinated Modeling Center (CCMC).

References

Brueckner, G. E., et al. (1995), The Large Angle Spectroscopic Coronagraph (LASCO), *Solar Phys.*, *162*, 357–402, doi:10.1007/BF00733434.

Canfield, R. C., K. P. Reardon, K. D. Leka, K. Shibata, T. Yokoyama, and M. Shimojo (1996), H alpha surges and X-ray jets in AR 7260, *Atrophys. J.*, *464*, 1016, doi:10.1086/177389.

Cirtain, J. W., et al. (2007), Evidence for Alfvén waves in solar X-ray jets, *Science*, *318*, 1580, doi:10.1126/science.1147050.

Corti, G., G. Poletto, S. T. Suess, R. L. Moore, and A. C. Sterling (2007), Cool-plasma jets that escape into the outer corona, *Astrophys. J.*, *659*, 1702–1712, doi:10.1086/512233.

De Moortel, I., S. W. McIntosh, J. Threlfall, C. Bethge, and J. Liu (2014), Potential evidence for the onset of Alfvénic turbulence in trans-equatorial coronal loops, *Astrophys. J. Lett.*, *782*(2), L34, doi:10.1088/2041-8205/782/2/L34.

Eyles, C. J., G. M. Simnett, M. P. Cooke, B. V. Jackson, A. Buffington, P. P. Hick, N. R. Waltham, J. M. King, P. A. Anderson, and P. E. Holladay (2003), The Solar Mass Ejection Imager (SMEI), *Solar Phys.*, *217*, 319–347, doi:10.1023/B:SOLA-0000006903-75671-49.

Filippov, B., L. Golub, and S. Koutchmy (2009), X-Ray jet dynamics in a polar coronal hole region, *Solar Phys.*, *254*, 259–269, doi:10.1007/s11207-008-9305-6.

Glesener, L., S. Krucker, and R. P. Lin (2012), Hard X-ray observations of a jet and accelerated electrons in the corona, *Astrophys. J.*, *754*, 9, doi:10.1088/0004-637X/754/1/9.

Golub, L., et al. (2007), The X-ray telescope (XRT) for the Hinode mission, *Solar Phys.*, *243*, 63–86, doi:10.1007/s11207-007-0182-1.

Heyvaerts, J., E. R. Priest, and D. M. Rust (1977), An emerging flux model for the solar flare phenomenon, *Atrophys. J.*, *216*, 123–137, doi:10.1086/155453.

Hick, P., A. Buffington, and B. V. Jackson (2005), The SMEI real-time data pipeline: From raw CCD frames to photometrically accurate full-sky maps, *Proc. SPIE*, *5901*, 59011B, doi:10.1117/12.617996.

Hick, P., A. Buffington, and B. V. Jackson (2007), A procedure for fitting point sources in SMEI white-light full-sky maps, *Proc. SPIE*, *6689*, 66890C.

Hollweg, J. V. (1981), Alfvén waves in the solar atmosphere. II: Open and closed magnetic flux tubes, *Solar Phys.*, *70*, 25–66.

Hollweg, J. V. (1982), Heating of the corona and solar wind by switch-on shocks, *Atrophys. J.*, *254*, 806–813, doi:10.1086/159791.

Hollweg, J. V. (1992), Alfvénically driven slow shocks in the solar chromosphere and corona, *Atrophys. J.*, *389*, 731–738, doi:10.1086/171246.

Hollweg, J. V., S. Jackson, and D. Galloway (1982), Alfvén waves in the solar atmosphere. III: Nonlinear waves on open flux tubes, *Solar Phys.*, *75*, 35–61.

Horn, B. K. P., and B. G. Schunck (1981), Determining optical flow, *Arti. Intell.*, *17*(1–3), 185–203, doi:10.1016/0004-3702(81)90024-2.

Howard, R. A., et al. (2008), Sun Earth Connection Coronal and Heliospheric Investigation (SECCHI), *Space Sci. Rev.*, *136*, 67–115, doi:10.1007/s11214-008-9341-4.

Huang, Z., M. S. Madjarska, J. G. Doyle, and D. A. Lamb (2012), Coronal hole boundaries at small scales. IV. SOT view. Magnetic field properties of small-scale transient brightenings in coronal holes, *Astron. Astrophys.*, *548*, A62, doi:10.1051/0004-6361/201220079.

Isobe, H., T. Miyagoshi, K. Shibata, and T. Yokoyama (2005), Filamentary structure on the Sun from the magnetic Rayleigh-Taylor instability, *Nature*, *434*, 478–481, doi:10.1038/nature03399.

Jackson, B. V., and P. P. Hick (1996), Coronal velocity determination using two-dimensional correlation techniques, *Eos Trans. AGU*, *77*(46 Supplement, F562).

Jackson, B. V., P. P. Hick, R. Howard, and K. Dere (1998), Two-dimensional correlation of LASCO images—Speeds derived for the background solar wind, *Eos Trans. AGU*, *79*, S275.

Jackson, B. V., A. Buffington, and P. P. Hick (2001), A heliospheric imager for solar orbiter, in *Solar Encounter: The First Solar Orbiter Workshop*, edited by B. Battrick and H. Sawaya-Lacoste, pp. 251–256, ESA Publications Division, Noordwijk, Netherlands.

Jackson, B. V., P. P. Hick, and A. Buffington (2003), Time-dependent tomography of heliospheric features using the three-dimensional reconstruction techniques developed for the solar mass ejection imager (SMEI), *Proc. SPIE*, *4853*, 23–30.

Jackson, B. V., et al. (2004), The Solar Mass-Ejection Imager (SMEI) mission, *Solar Phys.*, *225*, 177–207, doi:10.1007/s11207-004-2766-3.

Jackson, B. V., A. Buffington, P. P. Hick, X. Wang, and D. Webb (2006), Preliminary three-dimensional analysis of the heliospheric response to the 28 October 2003 CME using SMEI white-light observations, *J. Geophys. Res.*, *111*, A04S91, doi:10.1029/2004JA010942.

Jackson, B. V., M. M. Bisi, P. P. Hick, A. Buffington, J. M. Clover, and W. Sun (2008), Solar mass ejection imager 3-D reconstruction of the 27–28 May 2003 coronal mass ejection sequence, *J. Geophys. Res.*, *113*, A00A15, doi:10.1029/2008JA013224.

Jackson, B. V., P. P. Hick, A. Buffington, M. M. Bisi, J. M. Clover, and M. Tokumaru (2010), Solar Mass Ejection Imager (SMEI) and Interplanetary Scintillation (IPS) 3D-reconstructions of the inner heliosphere, *Adv. Geosci.*, *21*, 339.

Jackson, B. V., M. S. Hamilton, P. P. Hick, A. Buffington, M. M. Bisi, J. M. Clover, M. Tokumaru, and K. Fujiki (2011a), Solar Mass Ejection Imager (SMEI) 3-D reconstruction of density enhancements behind interplanetary shocks: In-situ comparison near Earth and at STEREO, *J. Atmos. Sol. Terr. Phys.*, *73*, 1317–1329, doi:10.1016/j.jastp.2010.11.023.

Jackson, B. V., M. Shimojo, K. Schenk, M. Tokumaru, and J. B. Gurman (2011b), HOP-187: Tracking X-ray jets from the solar surface to interplanetary space, *Hinode Observing Proposal (HOP) 187*.

Jackson, B. V., H.-S. Yu, A. Buffington, and P. P. Hick (2014), The dynamic character of the polar solar wind, *Atrophys. J.*, *793*(1), 54, doi:10.1088/0004-637X/793/1/54.

Jiang, Y. C., H. D. Chen, K. J. Li, Y. D. Shen, and L. H. Yang (2007), The Hα surges and EUV jets from magnetic flux emergences and cancellations, *Astron. Astrophys.*, *469*, 331–337, doi:10.1051/0004-6361:20053954.

Karpen, J. T., S. K. Antiochos, R. B. Dahlburg, and D. S. Spicer (1993), The Kelvin-Helmholtz instability in photospheric flows—Effects of coronal heating and structure, *Atrophys. J.*, *403*, 769–779, doi:10.1086/172248.

Kohl, J. L., et al. (1998), UVCS/SOHO empirical determinations of anisotropic velocity distributions in the solar corona, *Astrophys. J. Lett.*, *501*, L127, doi:10.1086/311434.

Kojima, M., and T. Kakinuma (1987), Solar cycle evolution of solar wind speed structure between 1973 and 1985 observed with the interplanetary scintillation method, *J. Geophys. Res.*, *92*, 7269–7279, doi:10.1029/JA092iA07p07269.

Kosugi, T., et al. (2007), The Hinode (Solar-B) mission: An overview, *Solar Phys.*, *243*, 3–17, doi:10.1007/s11207-007-9014-6.

Krieger, A. S., G. S. Vaiana, and L. P. van Speybroeck (1971), The X-ray corona and the photospheric magnetic field, in *Solar Magnetic Fields*, vol. 43, edited by R. Howard, pp. 397, International Astronomical Union, D. Reidel, Dordrecht, Netherlands.

Landi, S., P. Hellinger, and M. Velli (2006), Heliospheric magnetic field polarity inversions driven by radial velocity field structures, *Geophys. Res. Lett.*, *33*, L14101, doi:10.1029/2006GL026308.

Lee, L. C., and B. H. Wu (2000), Heating and acceleration of protons and minor ions by fast shocks in the solar corona, *Atrophys. J.*, *535*, 1014–1026, doi:10.1086/308879.

Lemen, J. R., et al. (2012), The Atmospheric Imaging Assembly (AIA) on the Solar Dynamics Observatory (SDO), *Solar Phys.*, *275*, 17–40, doi:10.1007/s11207-011-9776-8.

Liu, J., S. W. McIntosh, I. De Moortel, J. Threlfall, and C. Bethge (2014), Statistical evidence for the existence of Alfvénic turbulence in solar coronal loops, *Atrophys. J.*, *797*, 7, doi:10.1088/0004-637X/797/1/7.

Liu, W., T. E. Berger, A. M. Title, T. D. Tarbell, and B. C. Low (2011), Chromospheric jet and growing "loop" observed by Hinode: New evidence of fan-spine magnetic topology resulting from flux emergence, *Atrophys. J.*, *728*, 103, doi:10.1088/0004-637X/728/2/103.

Manoharan, P. K. (2010), Ooty interplanetary scintillation—Remote-sensing observations and analysis of coronal mass ejections in the heliosphere, *Solar Phys.*, *265*, 137–157, doi:10.1007/s11207-010-9593-5.

McComas, D. J., S. J. Bame, P. Barker, W. C. Feldman, J. L. Phillips, P. Riley, and J. W. Griffee (1998a), Solar Wind Electron Proton Alpha Monitor (SWEPAM) for the Advanced Composition Explorer, *Space Sci. Rev.*, *86*, 563–612.

McComas, D. J., et al. (1998b), Ulysses' return to the slow solar wind, *Geophys. Res. Lett.*, *25*, 1–4, doi:10.1029/97GL03444.

McComas, D. J., B. L. Barraclough, H. O. Funsten, J. T. Gosling, E. Santiago-Muñoz, R. M. Skoug, B. E. Goldstein, M. Neugebauer, P. Riley, and A. Balogh (2000), Solar wind observations over Ulysses' first full polar orbit, *J. Geophys. Res.*, *105*, 10,419–10,434, doi:10.1029/1999JA000383.

McComas, D. J., H. A. Elliott, J. T. Gosling, D. B. Reisenfeld, R. M. Skoug, B. E. Goldstein, M. Neugebauer, and A. Balogh (2002), Ulysses' second fast-latitude scan: Complexity near solar maximum and the reformation of polar coronal holes, *Geophys. Res. Lett.*, *29***(9)**, 1290, doi:10.1029/2001GL014164.

McComas, D. J., R. W. Ebert, H. A. Elliott, B. E. Goldstein, J. T. Gosling, N. A. Schwadron, and R. M. Skoug (2008), Weaker solar wind from the polar coronal holes and the whole Sun, *Geophys. Res. Lett.*, *35*, L18103, doi:10.1029/2008GL034896.

McIntosh, S. W., and B. De Pontieu (2012), Estimating the "dark" energy content of the solar corona, *Atrophys. J.*, *761*, 138, doi:10.1088/0004-637X/761/2/138.

Mizuno, D. R., et al. (2005), Very high altitude aurora observations with the Solar Mass Ejection Imager, *J. Geophys. Res.*, *110*, A07230, doi:10.1029/2004JA010689.

Moreno-Insertis, F., K. Galsgaard, and I. Ugarte-Urra (2008), Jets in coronal holes: Hinode observations and three-dimensional computer modeling, *Astrophys. J. Lett.*, *673*, L211–L214, doi:10.1086/527560.

Munro, R. H., and B. V. Jackson (1977), Physical properties of a polar coronal hole from 2 to 5 solar radii, *Atrophys. J.*, *213*, 874, doi:10.1086/155220.

Neugebauer, M. (2012), Evidence for polar X-ray jets as sources of microstream peaks in the solar wind, *Atrophys. J.*, *750*, 50, doi:10.1088/0004-637X/750/1/50.

Nisticò, G., V. Bothmer, S. Patsourakos, and G. Zimbardo (2009), Characteristics of EUV coronal jets observed with STEREO/SECCHI, *Solar Phys.*, *259*, 87–108, doi:10.1007/s11207-009-9424-8.

Nisticò, G., V. Bothmer, S. Patsourakos, and G. Zimbardo (2010), Observational features of equatorial coronal hole jets, *Ann. Geophys.*, *28*, 687–696, doi:10.5194/angeo-28-687-2010.

Pariat, E., S. K. Antiochos, and C. R. DeVore (2009), A model for solar polar jets, *Atrophys. J.*, *691*, 61–74, doi:10.1088/0004-637X/691/1/61.

Phillips, J. L., A. Balogh, S. J. Bame, B. E. Goldstein, J. T. Gosling, J. T. Hoeksema, D. J. McComas, M. Neugebauer, N. R. Sheeley Jr., and Y.-M. Wang (1994), Ulysses at 50 deg south: Constant immersion in the high-speed solar wind, *Geophys. Res. Lett.*, *21*, 1105–1108, doi:10.1029/94GL01065.

Phillips, J. L., et al. (1995), Ulysses solar wind plasma observations from pole to pole, *Geophys. Res. Lett.*, *22*, 3301–3304, doi:10.1029/95GL03094.

Raouafi, N.-E., and G. Stenborg (2014), Role of transients in the sustainability of solar coronal plumes, *Atrophys. J.*, *787*, 118, doi:10.1088/0004-637X/787/2/118.

Raouafi, N.-E., G. J. D. Petrie, A. A. Norton, C. J. Henney, and S. K. Solanki (2008), Evidence for polar jets as precursors of polar plume formation, *Astrophys. J. Lett.*, *682*, L137–L140, doi:10.1086/591125.

Savcheva, A., et al. (2007), A study of polar jet parameters based on Hinode XRT observations, *Publ. Astron. Soc. Jpn.*, *59*, 771.

Scherrer, P. H., et al. (2012), The Helioseismic and Magnetic Imager (HMI) investigation for the Solar Dynamics Observatory (SDO), *Solar Phys.*, *275*, 207–227, doi:10.1007/s11207-011-9834-2.

Schmieder, B., V. Archontis, and E. Pariat (2014), Magnetic flux emergence along the solar cycle, *Space Sci. Rev.*, *186*, 227–250.

Schmieder, B., Y. Guo, F. Moreno-Insertis, G. Aulanier, L. Yelles Chaouche, N. Nishizuka, L. K. Harra, J. K. Thalmann, S. Vargas Dominguez, and Y. Liu (2013), Twisting solar coronal jet launched at the boundary of an active region, *Astron. Astrophys.*, *559*, 1, doi:10.1051/0004-6361/201322181.

Shibata, K. (1982), Two types of jets and origin of macrospicules, *Solar Phys.*, *81*, 9–17, doi:10.1007/BF00151974.

Shibata, K., et al. (1992), Observations of X-ray jets with the YOHKOH Soft X-ray telescope, *Publ. Astron. Soc. Jpn.*, *44*, L173–L179, doi:10.1002/app.1992.070440119.

Shimojo, M., and K. Shibata (2000), Physical parameters of solar X-ray jets, *Atrophys. J.*, *542*, 1100–1108, doi:10.1086/317024.

Shimojo, M., and S. Tsuneta (2009), The relation between magnetic fields and coronal activities in the polar coronal hole, *Astrophys. J. Lett.*, *706*, L145–L149, doi:10.1088/0004-637X/706/1/L145.

Shimojo, M., S. Hashimoto, K. Shibata, T. Hirayama, H. S. Hudson, and L. W. Acton (1996), Statistical study of solar X-ray jets observed with the YOHKOH soft X-ray telescope, *Publ. Astron. Soc. Jpn.*, *48*, 123–136.

Sterling, A. C., R. L. Moore, D. A. Falconer, and M. Adams (2015), Small-scale filament eruptions as the driver of X-ray jets in solar coronal holes, *Nature*, *523*, 437–440, doi:10.1038/nature14556.

Threlfall, J., I. De Moortel, S. W. McIntosh, and C. Bethge (2013), First comparison of wave observations from CoMP and AIA/SDO, *Astron. Astrophys.*, *556*, 124, doi:10.1051/0004-6361/201321782.
Tian, H., S. W. McIntosh, S. R. Habbal, and J. He (2011), Observation of high-speed outflow on plume-like structures of the quiet Sun and coronal holes with Solar Dynamics Observatory/Atmospheric Imaging Assembly, *Atrophys. J.*, *736*, 130, doi:10.1088/0004-637X/736/2/130.
Tokumaru, M., M. Kojima, K. Fujiki, K. Maruyama, Y. Maruyama, H. Ito, and T. Iju (2011), A newly developed UHF radio telescope for interplanetary scintillation observations: Solar wind imaging facility, *Radio Sci.*, *46*, RS0F02, doi:10.1029/2011RS004694.
Tomczyk, S., and S. W. McIntosh (2009), Time-distance seismology of the solar corona with CoMP, *Atrophys. J.*, *697*, 1384–1391, doi:10.1088/0004-637X/697/2/1384.
Tomczyk, S., S. W. McIntosh, S. L. Keil, P. G. Judge, T. Schad, D. H. Seeley, and J. Edmondson (2007), Alfvén waves in the solar corona, *Science*, *317*, 1192.
Tomczyk, S., G. L. Card, T. Darnell, D. F. Elmore, R. Lull, P. G. Nelson, K. V. Streander, J. Burkepile, R. Casini, and P. G. Judge (2008), An instrument to measure coronal emission line polarization, *Solar Phys.*, *247*, 411–428, doi:10.1007/s11207-007-9103-6.
Tsuneta, S., et al. (2008), The magnetic landscape of the Sun's polar region, *Atrophys. J.*, *688*, 1374–1381, doi:10.1086/592226.
Vaiana, G. S., A. S. Krieger, L. Van Speybroeck, and T. Zehnpfennig (1970), Discovery of bright points (Entdeckung der hellen Flecken), *Bull. Am. Phys. Soc.*, *15*, 611.
Wang, Y.-M., N. R. Sheeley Jr., D. G. Socker, R. A. Howard, G. E. Brueckner, D. J. Michels, D. Moses, O. C. S. Cyr, A. Llebaria, and J.-P. Delaboudinière (1998), Observations of correlated white-light and extreme-ultraviolet jets from polar coronal holes, *Atrophys. J.*, *508*, 899–907, doi:10.1086/306450.
Wilhelm, K., et al. (2011), Morphology, dynamics and plasma parameters of plumes and inter-plume regions in solar coronal holes, *Astron. Astrophys. Rev.*, *19*, 35.
Yamauchi, Y., R. L. Moore, S. T. Suess, H. Wang, and T. Sakurai (2004), The magnetic structure of Hα macrospicules in solar coronal holes, *Atrophys. J.*, *605*, 511–520, doi:10.1086/381240.
Yang, S., J. Zhang, T. Li, and Y. Liu (2011), SDO observations of magnetic reconnection at coronal hole boundaries, *Astrophys. J. Lett.*, *732*, L7, doi:10.1088/2041-8205/732/1/L7.
Yokoyama, T., and K. Shibata (1995), Magnetic reconnection as the origin of X-ray jets and Hα surges on the Sun, *Nature*, *375*, 42–44, doi:10.1038/375042a0.
Yokoyama, T., and K. Shibata (1996), Numerical simulation of solar coronal X-ray jets based on the magnetic reconnection model, *Publ. Astron. Soc. Jpn.*, *48*, 353–376.
Yu, H.-S., B. V. Jackson, A. Buffington, P. P. Hick, M. Shimojo, and N. Sako (2014), The three-dimensional analysis of Hinode polar jets using images from LASCO C2, the STEREO COR2 coronagraphs, and SMEI, *Atrophys. J.*, *784*, 166, doi:10.1088/0004-637X/784/2/166.